

1 **Causality and Time-Lagged Dependencies at the Watershed Scale**

2 **K. G. Calixto¹, J. V. Coutinho¹, and E. C. Wendland¹**

3 ¹ São Carlos School of Engineering, University of São Paulo.

4 Corresponding author: Kalyl Gomes Calixto (kalyl.calixto@gmail.com)

5 **Key Points:**

- 6 • Synthetic time series and hydrologic data from a small-sized watershed are examined
7 using causal inference methods
- 8 • Medium-term patterns of lagged dependencies between streamflow, groundwater levels,
9 and meteorological variables are found
- 10 • Improved hydrologic system understanding has the potential to benefit the evaluation and
11 development of predictive tools
- 12

Abstract

Investigating watershed hydrology from a data-driven causal perspective consists of an attractive opportunity to characterize and understand relationships between water storages and fluxes. Previous studies have focused on assessing causal interactions of individual hydrologic processes along with their environmental drivers. Here we assess integrally how the water balance components interact with themselves, aiming to find relevant time-lags or dependency patterns. Granger's causality test and time-lagged mutual information were used in a pairwise approach to examine cause-effect relationships between precipitation, streamflow, groundwater levels under different land-covers, and evapotranspiration data (daily timescale) from 2009 to 2019 in a Brazilian watershed (52 km²), located in a recharge area of the Guarani Aquifer System. A verification assessment using synthetic datasets shows that the methods are effective to identify the underlying generating mechanisms. Statistically significant causal connections were confirmed in practically all pairs of observed data. Granger's causality indicates that groundwater and streamflow responses are influenced by precipitation even with a lag of 1-day ("instantaneous interaction"), while the evapotranspiration can take more than 200 days to influence groundwater responses, depending on the water table depth and surrounding land-cover. From the mutual information curves, the first local peaks are possibly associated with a physical mechanism, while other peaks, despite resulting statistically significant, lack a reasonable interpretation and require further research. The causal analysis provides a complementary view of the hydrological system's functioning and challenges us to develop predictive models that reproduce not only the target variables but also the diverse time-lagged dependencies observed in environmental data.

35

Plain Language Summary

The amount of water moving between the atmosphere, plants, soil, aquifers, and surfaces is continuously changing over time. Hydrologists are interested to understand and quantify these changes, associating them to the environmental conditions. In hydrology, observational datasets from natural systems are the main source of information. Here we characterize the temporal dependencies between rainfall, streamflow, groundwater levels, and evaporation rates observed in a recharge area of the Guarani Aquifer System. Instead of methods based on correlation, we applied techniques capable to find, in a broader way, how past observations help to predict current processes. We identify the time variability and strength of time-lagged dependencies and confirm the existence of causal connections. While a physical interpretation of part of the statistical results was possible, further studies are needed to take advantage of the information obtained. Applying causal analysis in hydrology, just like in other science fields (Earth sciences, ecology, neuroscience), is interesting because it provides us with additional knowledge of the underlying systems and has the potential to improve the consistency, quality, and value of our predictions. Reliable projections of the possible futures will help us to be better prepared for threatening situations.

52

53

54

55

56 **1 Introduction**

57 Applying causal inference methods in hydrology finds motivation in the complexity of
58 the multiple interactions and interdependencies between hydrological, climatic, environmental,
59 and human systems, in both space and time domains (Kumar, 2015). The analysis of
60 observational data, which are becoming increasingly available from satellite remote sensing,
61 station-based, and field site measurements (Runge et al., 2019), has been one of the most feasible
62 alternatives to investigate hydrological variability and causality (Blöschl et al., 2019; Ombadi et
63 al., 2020). Mechanisms of how the water cycle components are being impacted by natural and
64 human-induced changes, including climate change, land-use changes, and increasing water
65 demands, may be unraveled with causal frameworks (Goodwell et al., 2020). Similarly, the
66 environmental conditions that control hydrologic responses of interest for management purposes
67 (e.g., extreme events) can be better understood (Pelletier and Tucotte, 1997; Dey and Mujumdar,
68 2018).

69 Ruddell and Kumar (2009) used transfer entropy (an information-theoretic statistical
70 measure) for quantifying several properties of information flow and interactions between pairs of
71 variables measured at an eddy flux tower. Goodwell and Kumar (2017) investigated complex
72 dependencies and proposed a partitioning method to characterize how two source variables
73 jointly influence a third (target) variable. The results were illustrated with an application to data
74 measured at a weather station. In more recent applications of causal methods in hydrology:
75 Ombadi et al. (2020) compared four methods (Granger causality, transfer entropy, PC algorithm,
76 and convergent cross mapping) and examined pairwise causal relationships in the
77 evapotranspiration process using data from a flux tower; Franzen et al. (2020) characterized
78 time-lagged dependencies between precipitation and streamflow data observed in a large river
79 basin using mutual information; and Bennett et al. (2019) used a lag 1-day transfer entropy to
80 quantify and compare the intensity of interaction between simulated hydrologic data.

81 As suggested by the scope of related studies, applications in which the underlying
82 causality mechanisms are reasonably well-known represent opportunities to test and explore
83 causal methods before moving to the analysis of more complex interactions. To date, no studies
84 have focused on an exploratory and comprehensive causal analysis in a monitored watershed
85 aiming to quantify the time-lagged dependencies between precipitation, evapotranspiration,
86 streamflow, groundwater levels, and vegetation indices data, not even in a simple pairwise setup.

87 As prediction is one of the main goals of science, the presence of properties in time series
88 data that facilitate to predict future terms from past observed behavior and patterns has a
89 fundamental value. Memory and persistence (dependences between past and future states) are
90 properties widely found in hydrologic data. Hurst was the precursor in identifying that the
91 hypothesis of serial independence of hydrological data results in statistical inconsistencies,
92 triggering a series of studies that formalized the theory of long memory processes (Amblard &
93 Michel, 2013; Graves et al., 2017). As practical examples, Zimmermann et al. (2006) and
94 Tomasella et al. (2008) identified significant memory effects in studies related to deforestation
95 and interannual variability of precipitation in the Amazon rainforest, suggesting that the history
96 of land-use and the groundwater system were influencing later hydrological responses. To detect
97 such cause and effect relationships from observational data, several methods have been
98 developed (e.g., Granger's method and variations, causal maps, causal networks, algorithms
99 based on information theory) (Runge et al., 2019). The selection of the most appropriate method

100 depends on the prior knowledge of the system, on the nature of the variables involved and on the
101 intended objectives.

102 The Granger causality test has been one of the most used statistical tools to determine the
103 presence of causal relationships between random variables (Barnett & Seth, 2015).
104 Papagiannopoulou et al. (2017), McGraw and Barnes (2018), Singh and Borrok (2019) and
105 Huang et al. (2019) applied the test to investigate, respectively, the dynamics between climate
106 and vegetation, the climate variability, the association between groundwater reserves and food
107 production on a global scale, and the dependence between climatic and hydrological variables.
108 The advantage of the method proposed by Granger (1969) over traditional methods based on
109 correlations or regressions with lagged explanatory variables is the consideration of the memory
110 effects of the response variables (McGraw & Barnes, 2018). Granger (1969) proposed that a
111 process S causes, in Granger's sense, another process, T , if future values of T can be better
112 predicted using values of S and T instead of just values of T . An assumption of the classic
113 Granger causality test is the linearity premise for the underlying system. Despite that, some
114 studies have reported the capability to detect, with some limitations, even nonlinear interactions
115 (Barnett & Seth, 2014; Ombadi et al., 2020).

116 Along with the Granger test, methods derived from the information theory (IT) – which
117 are based on the entropy measure (Shannon, 1948) and operate on probability distribution
118 functions (pdf) – are attracting increasing attention in hydrologic research and Earth system
119 sciences (Weijs et al., 2010; Rinderer et al., 2018; Goodwell et al., 2020; Kumar & Gupta, 2020).
120 The principal reasons are found in the capability of information-theoretic methods to provide us
121 with stronger and more robust conclusions with respect to data interaction and connectivity
122 (Ruddell & Kumar, 2009; Goodwell & Kumar, 2017; Jiang & Kumar, 2019). Moreover, the
123 methods do not rely on specific data properties or on the nature of dependencies (linear or
124 nonlinear). Data limitations – for instance, significant changing behaviors (Ombadi et al., 2020)
125 and insufficient sample lengths (Li et al., 2018) – still hinder the application of IT methods.

126 Two specific measures based on informational entropy have been widely applied for
127 causal inference: time-lagged mutual information (TLMI) and transfer entropy (TE). The first,
128 TLMI, is a more practicable approach, which measures the general dependence (linear and
129 nonlinear) between two variables (Fraser & Swinney, 1986), and requires considerably shorter
130 sample lengths of data. TLMI is not capable to eliminate data memory effects (like the Granger
131 causality test does) so that static dependencies are not ignored (Li et al., 2018). To address this
132 limitation, Schreiber (2000) proposed the transfer entropy (TE), a conditioned mutual
133 information, which measures the amount of directional information transferred between
134 variables, excluding those memory effects induced by the response (target) time series. Barnett et
135 al. (2009) demonstrated that the TE metric is proportional to the likelihood ratio of the Granger
136 causality test for Gaussian random variables. Despite the advantages, the estimation of TE is still
137 a challenging problem and an active area of research, due to numerical issues, high
138 dimensionality (determined by the number of time lags between the variables), and dependence
139 on accurate estimates of probability distributions (Gençağa, 2018).

140 Here we explore time-lagged dependencies between hydrologic variables measured in a
141 small watershed. The Granger causality test and the normalized time-lagged mutual information
142 metric (NMI) were selected to perform this study due to their suitability to assess the
143 connectivity and dependency throughout long time windows. We expected to find patterns of
144 interactions and estimate memory time scales associated with the hydrological processes, which

145 may support, directly or not, the predictive modeling and the system characterization. This study
146 represents an opportunity to identify the potentials and limitations of applying causal methods in
147 headwater or small watersheds, which are widely acknowledged for their importance in the
148 context of water management, and to discuss the innovative or relevant information we can
149 obtain from them.

150

151 **2 Materials and Methods**

152 **2.1 Study Area**

153 The study domain is limited to the Onça Creek watershed (OCW) (~65 km²), located in
154 an agricultural area of the state of São Paulo (Brazil) (47°54' – 48°00'W, and 22°09' – 22°15'S)
155 (Figure 1). The watershed entirely lies on a recharge area of the Guarani Aquifer System (GAS),
156 which is one of the most important groundwater reserves in South America, responsible for
157 supplying water to more than 90 million people in Argentina, Brazil, Paraguay, and Uruguay
158 (Araújo et al., 1999; Kirchheim et al., 2019).

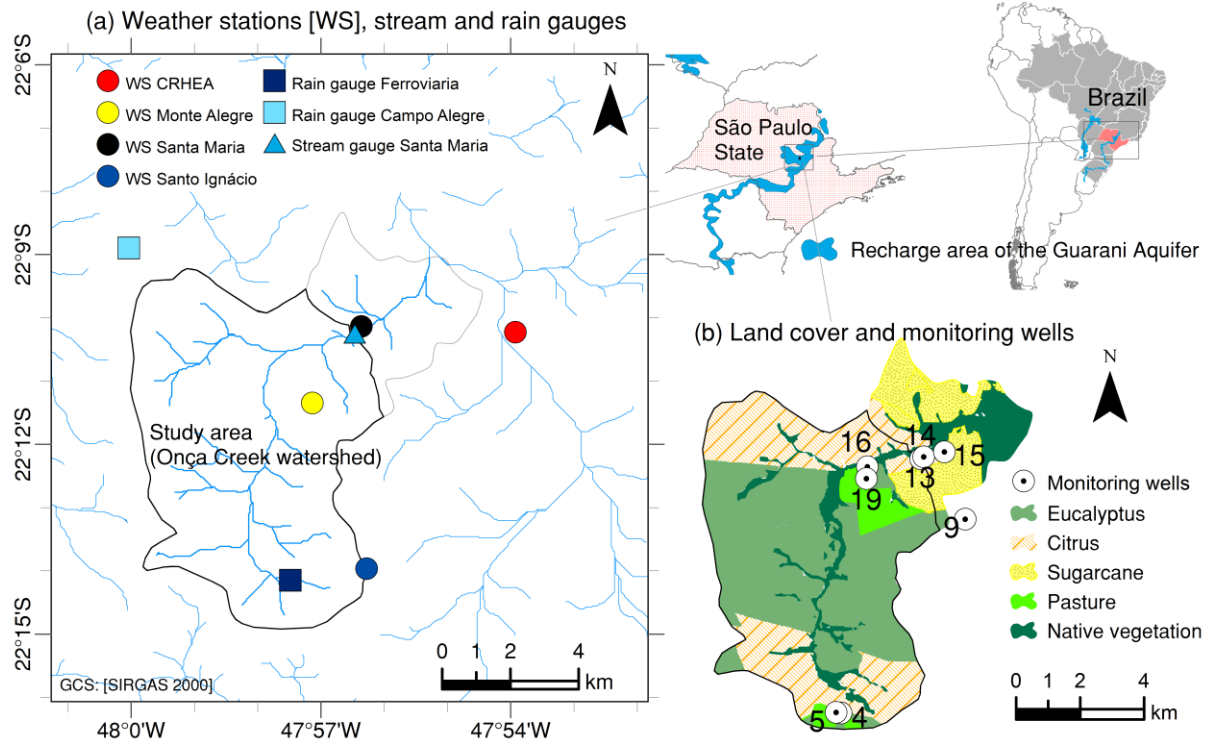
159 The GAS is composed of sandstone layers from the Jurassic (Botucatu Formation) and
160 Triassic (Piramboia Formation) periods and is widely (~ 90%) confined by basaltic spills that
161 occurred in the Cretaceous period (Serra Geral Formation). The study area, instead of presenting
162 such a confining layer, presents a permeable deposit of Cenozoic sediments with a thickness of
163 tens of meters, and a specific yield varying from 0.08 to 0.16 (Wendland et al., 2015; Coutinho et
164 al., 2020).

165 The watershed has an average terrain surface slope of 8 m/km, and elevations between
166 825 and 655 m above sea level (a.s.l.). Sandy soils, which dominate the watershed, along with
167 the mild surface slope favor the occurrence of high infiltration rates and low overland flow. The
168 Köppen-Geiger climate classification (Alvares et al., 2013) indicates a humid subtropical
169 climate, with dry winters and rainy summers (Cwa). From 1979 to 2014, the mean annual
170 precipitation was 1486 mm (about 65% in the rainy seasons), and the mean annual temperature,
171 21.6 °C (Cabrera et al., 2016).

172 Agricultural and livestock activities have dominated the area during the last decades. In
173 1990, eucalyptus plantations covered about 30% of the total area, pastures, 15%, and the native
174 vegetation (Cerrado, tropical savanna), 30% (Pompeo, 1990). In 2017, eucalyptus, citrus,
175 sugarcane, and pasture activities summed-up approximately 35%, 30%, 10%, and 4%,
176 respectively, with the remaining native vegetation corresponding to only 10% (Figure 1).

177 Data from the monitoring stations and wells indicated in Figure 1 were used in this study.
178 The reference period covered December 2008 to September 2019. Basic quality control
179 procedures were followed to ensure data consistency.

180



181
 182 **Figure 1.** Location of the study area. (a) hydrometeorological stations and (b) dominant land-
 183 covers and monitoring wells. Data sources: 1. Recharge areas of the Guarani Aquifer:
 184 <http://geoserver.ourinhos.unesp.br/>; 2. DEM: <https://www.infraestruturameioambiente.sp.gov.br/>

185

186 2.2 Streamflow and Baseflow Data

187 The discharge time series was estimated at the stream gauge Santa Maria, in a section that
 188 drains an area of 52.1 km² (Figure 1), and located immediately upstream to a crossroad with two
 189 culvert pipes with a diameter of 1.50 m. Discharge measurements have been carried out by
 190 current meters twice a month since 2004. The daily discharges (long-term mean = 0.65 m³/s)
 191 were estimated from the transformation of sub-hourly water level data, using the classic power-
 192 law stage-discharge transformation function. The level data are recorded every 15 minutes, since
 193 December 2008, by water level loggers maintained in a stilling well hydraulically connected to
 194 the stream. The parameter for zero flow condition was set based on the invert elevation of the
 195 culverts, while the other rating curves parameters were calculated by the ordinary least square
 196 method. The parameters are variable over time due to the channel section instability (sandy
 197 stream bed) and due to the downstream impoundment with controlled water release during the
 198 dry seasons. Considering the errors associated with the rating-curves and the water level data, the
 199 median uncertainty in the estimated discharges was 11.9%, whereas the mean uncertainty,
 200 13.0%.

201 The unconfined aquifer holds a high interaction with the stream, maintaining its perennial
 202 regime (Wendland et al., 2015). To estimate the daily baseflow time series, the two-parameter
 203 separation method proposed by Duncan (2019) was applied. This method comprises a backward
 204 filtering operation to fit an exponential master recession curve, followed by the original Lyne

205 and Hollick digital filter to smooth the resulting curve. The filter parameters in the first and
 206 second pass were set equal to 0.983. The baseflow index was estimated as 0.86, which is
 207 comparable to the value of 0.83 obtained by Batista et al. (2018) through isotopic mass balance
 208 calculations, in nearby catchments with similar meteorological and hydrogeological conditions
 209 (recharge areas of the GAS).
 210

211 2.3 Meteorological Data

212 The operation periods up to September 30, 2019, of the four nearby weather stations
 213 (WS, circles in Figure 1) and the two rain gauges (RG, squares in Figure 1) defined the
 214 meteorological datasets used here. All weather stations are equipped with rain gauges, air
 215 temperature and humidity probes, pyranometers, and anemometers.

216 Reference evapotranspiration rates were calculated by the Penman-Monteith method (PM
 217 FAO-56) (Allen et al., 1998). Given the dimensions of the study area and the spatial variability
 218 of meteorological variables, daily precipitation data and the reference evapotranspiration
 219 calculated at each WS were interpolated. The deterministic method of inverse distance weighting
 220 (IDW), with power 2 (Dirks et al., 1998), was used to obtain daily grid surfaces (50 x 50 m) from
 221 simultaneous records. The average values over the monitored drainage area formed the final time
 222 series of precipitation and reference evapotranspiration.
 223

224 2.4 Spectral Vegetation Indices and Evapotranspiration

225 The vegetation dynamics can be relevant to describe the hydrological behavior of
 226 catchments, especially in small spatial and temporal scales (Area < 500 km² and 1 - 5 years)
 227 (Donohue et al., 2007; Wegehenkel, 2009). Studies have shown that the relationships between
 228 actual (AET) and reference (RET) evapotranspiration are reasonably well estimated, in diverse
 229 biomes, as a function of remotely sensed vegetation indices (Glenn et al., 2008; Glenn et al.,
 230 2011; Kamble et al., 2013; Nagler et al., 2013).

231 The empirical method proposed by Nagler et al. (2013), based on experimental studies in
 232 the state of Arizona (USA), was adapted here to provide an estimate of the actual
 233 evapotranspiration. The method follows Equation 1, which is based on the Beer-Lambert law to
 234 determine the absorption of light by a canopy and takes the enhanced vegetation index (EVI) as
 235 an indicator of the density of light-absorbing particles.
 236

$$\text{AET} = [a(1 - \exp(-b \cdot \text{EVI})) - c] \times \text{RET}$$

1)

237 in a , b , and c are parameters to be calibrated against observed data. As a simplification,
 238 motivated by the lack of observed evapotranspiration in the study area (e.g., by flux towers in
 239 representative land covers), we adopted $a = 1.65$ and $b = 2.25$, the same values estimated by
 240 Nagler et al. (2013), and left c as a free parameter to be adjusted in the water balance assessment.
 241 This is equivalent to allow for slight translations in the transformation curve, maintaining the
 242 sensibility of the ratio AET/RET with respect to EVI.

243 The EVI data, referring to the surrounding areas of the monitoring wells and to the
 244 watershed area, were taken from the product MOD13Q1 (Didan, 2015), generated every 16 days
 245 in 250 m spatial resolution, and made available on the NASA Land Processes Distributed Active
 246 Archive Center (LP DAAC). Daily values of EVI were obtained from linear interpolation, then
 247 individual time series of actual evapotranspiration for each well and for the watershed were
 248 calculated.

249

250 2.5 Groundwater Level

251 The surrounding typical land covers, the ranges of water level variation of the eight
 252 monitoring wells considered in this study (Figure 1), and the respective specific yield (drainable
 253 porosity) values are shown in Table 1. The wells have been monitored every 15 days by water
 254 level meters, and twice a day by dataloggers (Levellogger® Edge 3001 or Diver® DI501). The
 255 datasets from the manual and automatic measurements were adjusted, resampled, and merged to
 256 form the final daily time series for each well. Also, an average groundwater level variable
 257 (named ‘GWL’) was defined as the arithmetic mean of the levels observed in the monitoring
 258 wells.

259

260 **Table 1.** Description of the groundwater monitoring wells (m b.g.l. = meters below ground
 261 level). Specific yield (drainable porosity) values were obtained from Wendland et al. (2015).

ID	Land cover	Water level depth (m b.g.l.)			Specific yield
		min	mean	max	
W4	Pasture	14.4	16.5	17.9	15.9%
W5	Pasture	3.6	6.3	9.1	15.9%
W9	Eucalyptus	15.6	20.2	24.4	15.1%
W13	Sugarcane	5.5	9.8	11.0	15.1%
W14	Sugarcane	2.8	6.6	7.6	15.1%
W15	Citrus	4.6	7.8	9.5	8.5%
W16	Eucalyptus	2.7	5.2	7.2	12.3%
W19	Eucalyptus	8.9	15.1	18.7	12.3%

262

263

264 2.6 Water Balance

265 We examined the water balance dynamics in the watershed from October 01st, 2009 to
 266 September 30th, 2019, which corresponds to ten complete water years in the study area. The
 267 control volume of inputs and outputs was defined as the region from the upper canopy layer to
 268 the layer where deep regional recharge (outflow to the GAS) occurs.

269

$$\Delta S = PP - AET - Q - DR \quad (2)$$

270 in which ΔS : water storage change, PP: precipitation, AET: actual evapotranspiration,
 271 Q: discharge, and DR: deep recharge. Based on the study by Wendland et al. (2007), the deep

272 recharge was assumed as 3.5% of the average annual precipitation (~ 50 mm/a in the study
 273 period). The accumulated water storage changes are supposed to follow the average behavior of
 274 the groundwater levels because the soil moisture has negligible annual variations in the study
 275 area (Pompeo, 1990).

276

277 2.7 Granger Causality Test (GC)

278 The Granger causality definition is based on the increase of predictive power of an
 279 autoregressive model by including an additional variable, candidate to present a causal
 280 relationship, with a certain time lag (Granger, 1969). Some considerations to make such
 281 definition applicable are that the data are generated according to a linear, Gaussian, and
 282 stationary autoregressive process. In the simplest, bivariate case, two models are considered: the
 283 unrestricted (Equation 3), with the past values of the variables X and Y; and the restricted
 284 (Equation 4), only with the past values of the variable Y.

285

$$y_{u_t} = c_u + \sum_{j=1}^p [\phi_{1j}y_{t-j} + \phi_{2j}x_{t-j}] + \epsilon_t, \quad \epsilon_t \sim N(0, v_u) \quad (3)$$

286

$$y_{r_t} = c_r + \sum_{j=1}^p \phi_{1j}y_{t-j} + \epsilon_t, \quad \epsilon_t \sim N(0, v_r) \quad (4)$$

287 in which c_u , c_r , ϕ_{1j} e ϕ_{2j} are model parameters, and ϵ_t is a Gaussian error, with variance v .

288 The null hypothesis is accepted when $\phi_{2j} = 0$ for $j = 1, 2, \dots, p$, meaning that X does not
 289 cause Y in the Granger sense. Conversely the null hypothesis is rejected when $\phi_{2j} \neq 0$ for a j
 290 between 1 and p .

291 The open source library Statsmodels 0.9.0 (Seabold & Perktold, 2010) was used for the
 292 computational implementation of the method. The algorithm executes the test for multiple time
 293 lags (up to the maximum lag length) between pairs of variables and examines the corresponding
 294 statistical significance of the causal relationships based on the likelihood ratio test (Equation 5).

295

$$LR = -2 \log \left[\frac{\mathcal{L}_r(\hat{\theta}_0)}{\mathcal{L}_u(\hat{\theta}_1)} \right] \sim \chi^2 \text{ (d.f. = } p_u - p_r \text{)} \quad (5)$$

296

297 in which LR is the likelihood ratio, $\hat{\theta}_i$ indicates the maximum likelihood estimation of θ_i (model
 298 parameters) under the hypothesis i , \mathcal{L} indicates the likelihood function, and the subscripts u and
 299 r refer to the unrestricted and restricted model, respectively. The LR follows approximately a
 300 chi-square distribution, with degrees of freedom (d.f.) equal to the difference between the
 301 number of parameters of the unrestricted (p_u) and restricted (p_r) models (Wilks, 1938).

302

303 2.8 Time-lagged normalized mutual information (NMI)

304 The mutual information $I(X; Y)$ is defined as the relative entropy between the joint
 305 distribution and the product distribution (Cover & Thomas, 2005):

306

$$I(X; Y) = \sum_{x \in \mathcal{X}} \sum_{y \in \mathcal{Y}} p_{XY}(x, y) \log_2 \frac{p_{XY}(x, y)}{p_X(x)p_Y(y)} = H(X) + H(Y) - H(X, Y) \quad (6)$$

307 in which p_X , p_Y and p_{XY} are marginal and joint probability mass functions, and $H(X)$, $H(Y)$ and
 308 $H(X, Y)$ are the entropy and joint entropy of the discrete random variables X and Y . The mutual
 309 information $I(X; Y)$ measures the general dependence (linear and non-linear) between two
 310 variables and can be seen as the reduction of the uncertainty of variable X (or Y) due to
 311 knowledge of variable Y (or X). By adopting some time lag between the variables under
 312 analysis, mutual information can be used to detect the direction and intensity of interaction
 313 between linear or non-linear processes (Li et al., 2018).

314

$$TLMI(X; Y, \tau) = - \sum \sum p_{XY}(x_t, y_{t+\tau}) \log_2 \frac{p_{XY}(x_t, y_{t+\tau})}{p_X(x_t)p_Y(y_{t+\tau})} \quad (7)$$

315 in which TLMI is the time-lagged mutual information, and τ is the time lag between the cause
 316 (X) and effect (Y) variable. A normalized metric, presented in Equation 8, was used here.

317

$$0 \leq NMI(X, Y; \tau) = \frac{TLMI(X, Y; \tau)}{\min[H(X), H(Y)]} \leq 1 \quad (8)$$

318 in which $H(X)$ and $H(Y)$ are the entropy of X and Y .

319 The marginal and joint probability distributions were estimated from histograms (Li et
 320 al., 2017). For each pair of variables (X , Y), the number of bins was set as the geometric average
 321 of the numbers individually determined by the Freedman-Diaconis rule (Freedman; Diaconis,
 322 1981).

323

324 2.9 Verification Assessment

325 The verification strategy presented here aimed to identify errors in the computational
 326 implementation and to understand the results for situations in which the temporal dependencies
 327 between cause and effect are well-known. Synthetic time series, generated according to
 328 Equation 9 (W_t , a simple summation function) and Equation 10 (Z_t , a discrete convolution
 329 operation), were investigated by both the Granger causality test and the normalized time-lagged
 330 mutual information.

331

$$W_t = \max \left(0; 0.20 + 1 \times 10^{-4} \times \sum_{j=-m}^m [PP_{t-\tau^*+j}]^a + \epsilon_t \right), \quad \epsilon_t \sim N(0, d^2 \sigma_{PP}^2) \quad (9)$$

332

$$Z_t = \sum_{j=-\infty}^{\infty} PP_{t-j} UH_j + \epsilon_t, \quad UH_t = \frac{(t/k)^{n-1} \exp(-t/k)}{k(n-1)!}, \quad E[UH_t] = n \cdot k; \quad \epsilon_t \sim N(0, d^2 \sigma_{PP}^2) \quad (10)$$

333 in which PP_t [mm] is the mean areal daily precipitation time series in the study area, σ_{PP} is the
 334 sample standard deviation of PP (~9 mm), $E[UH_t]$ is the expected value of the gamma
 335 distribution function UH_t (Besbes & de Marsily, 1984), and ϵ_t is an uncorrelated Gaussian noise.
 336 The parameter arrays, (a, m, τ^*, d) for W_t and (n, k, d) for Z_t , were set as shown in Table 2. The
 337 ranges intended to assess the methods under diverse conditions. The premise is that the methods
 338 were capable to identify the lags $L_W = \tau^*$ for W_t , and $L_Z = n \times k$ for Z_t .

339

340

341 **Table 2.** Parameters adopted to generate the W and Z synthetic time series.

Time series	Group ID	Fixed Parameters	Variable Parameter
W	1	$a = 1$ $d = 1$ $\tau^* = 200$ $m = 1$	$m_j = 1; 10; 100$
	2	$d = 1$ $\tau^* = 200$	$a_j = 0.1; 0.5; 2$
	3	$a = 1$ $m = 1$ $\tau^* = 200$	$d_j = 0.01; 0.10; 10$
	4	$a = 1$ $m = 1$ $d = 1$	$\tau_j^* = 200; 500; 800$
Z	1	$n = 10$ $d = 0.01$	$k_j = 10; 20; 30$
	2	$k = 10$ $d = 0.01$	$n_j = 5; 20; 30$
	3	$n = 14$ $k = 14$	$d_j = 0.001; 0.1; 1.0$

342

343

344 2.10 Analysis of Observed Data

345 The Granger causality test and the normalized lagged mutual information were calculated
 346 in a pairwise setup. The pairs were defined as: in a first set, precipitation and evapotranspiration
 347 as source ('cause') variables, whereas streamflow, baseflow, and groundwater level as target
 348 ('response') variables; and in a second set, reference evapotranspiration, enhanced vegetation
 349 index and groundwater level as sources, while streamflow and baseflow as targets. Incremental
 350 lags, from 1 up to 1000 days, were considered. These pairs were defined based on likely or

351 possible cause-effect relationships in the hydrological system. For example, it is expected that
352 precipitation directly influences groundwater levels and streamflow.

353 All the observed time series were affected by uncorrelated Gaussian noise to compensate
354 for uncertainties in the deterministic estimations of the hydrological processes. Due to data
355 insufficiency and for the purpose intended here, the statistical properties of errors were taken as
356 fixed approximations. A coefficient of variation (relative uncertainty) of 15% was adopted for
357 streamflow, baseflow, and evapotranspiration estimates, whereas fixed standard deviations of
358 10 mm, 0.02 m, and 0.06 were set for precipitation, groundwater level and EVI data,
359 respectively.

360 The statistical significance of the mutual information values was verified using a shuffled
361 surrogate method (Ruddell & Kumar, 2009; Franzen et al., 2020). In this method, the time series
362 data are shuffled to destroy time dependencies between the variables, and the mutual information
363 is calculated using both the shuffled and the original data. Thirty iterations of shuffled data were
364 used to compute a critical value associated with a 95% confidence level. Gaussian distribution
365 was assumed. When the mutual information calculated for the observed data is greater than the
366 critical value (calculated based on the shuffled sequences), the mutual information value is
367 considered statistically significant.

368

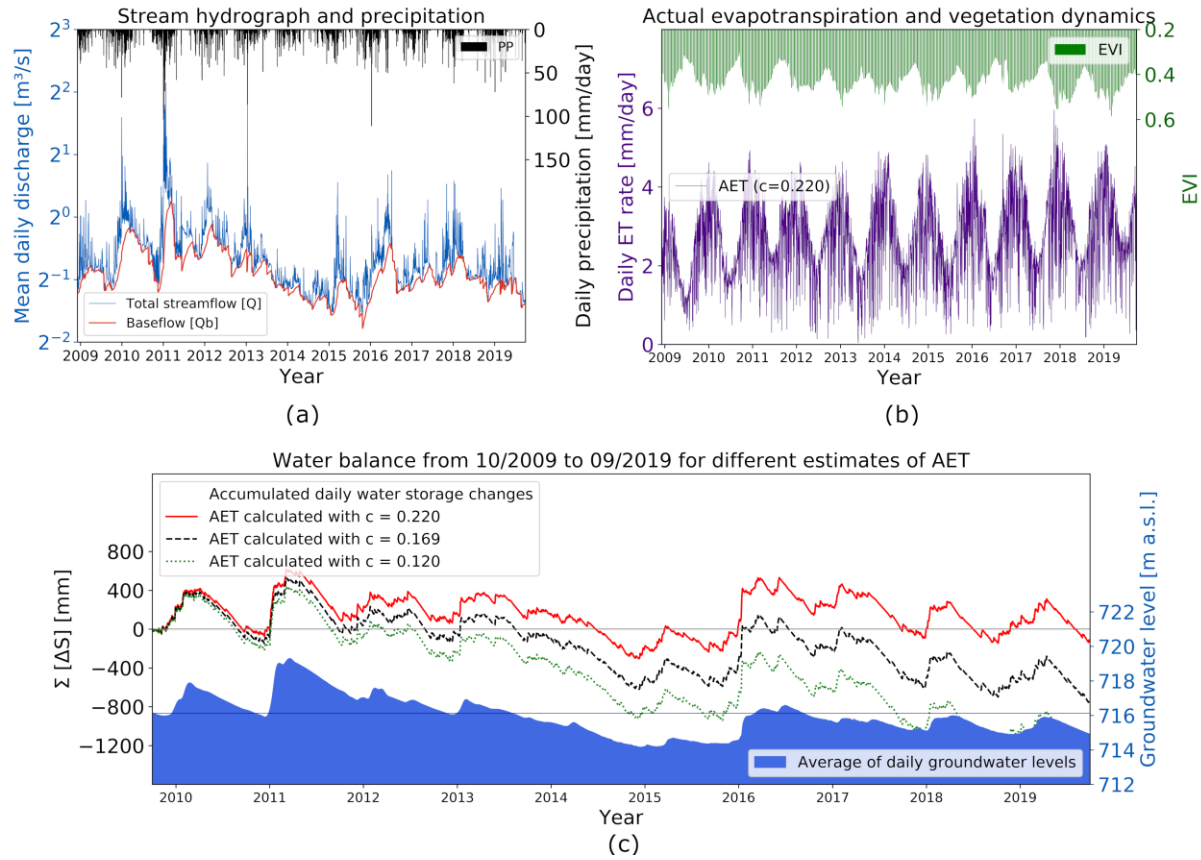
369 **3 Results**

370 **3.1 Water Balance Dynamics**

371 Figure 2 shows the time series from 2009 to 2019 of the streamflow (total, Q and
372 baseflow, Q_b), precipitation (PP), estimated actual evapotranspiration (AET), enhanced
373 vegetation index (EVI) and average groundwater level (GWL). There is a groundwater
374 dominance in the streamflow dynamics, with a baseflow index greater than 0.85. The ratio of
375 reference evapotranspiration by annual precipitation is 0.87, and the ratio of AET by annual
376 precipitation, 0.70. Trend analysis was not the focus here, however, it is possible to see a slight
377 downwards trend in Q, Q_b, and GWL time series data, and also an apparent upwards trend in the
378 AET.

379 The water year 2013-2014 was marked by a meteorological drought (Coelho et al., 2016;
380 Marengo et al., 2015), with annual precipitation 20% lesser than the average. The impacts on
381 groundwater levels and streamflow can be readily observed. Minimum groundwater levels were
382 reached in January 2015, and minimum streamflow, in September 2015.

383 From October 2009 to September 2019, the average groundwater level experienced a
384 reduction from 716.13 to 714.90 m a.s.l. Considering a mean specific yield of 0.10, this
385 groundwater level change represents a water storage reduction of 123 mm in the phreatic zone.
386 In the water balance, when the parameter *c* used to estimate the AET is taken as 0.220, the
387 accumulated water storage changes in the watershed varied from -4 to -125 mm in the same
388 period. This reasonable water balance closure suggests that the estimates presented in Figure 2
389 are consistent and can be used in our causal analyses.



390

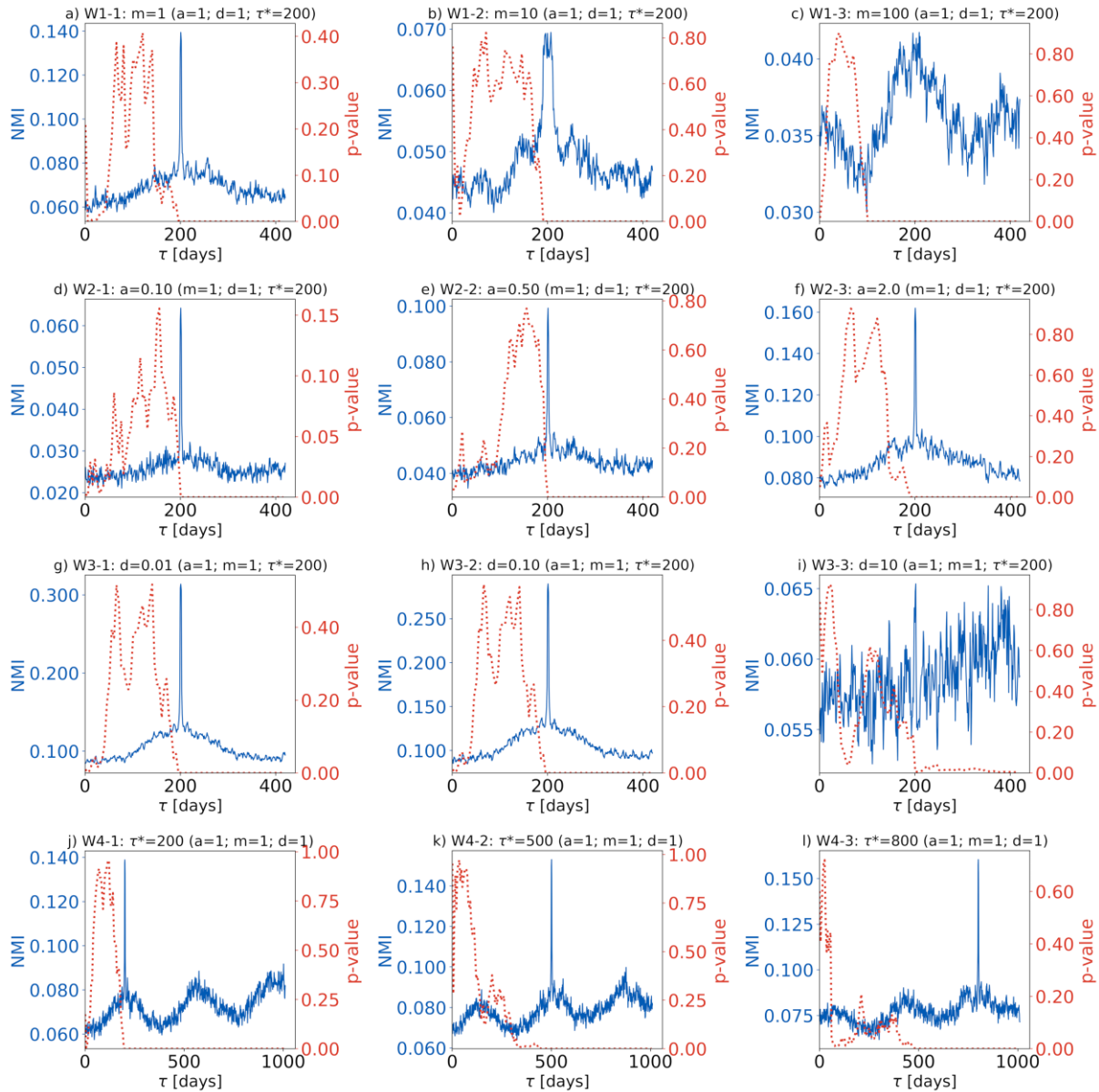
391 **Figure 2.** Water balance components and vegetation index time series in the study area. The
 392 actual evapotranspiration calculated with $c = 0.220$ (continuous red line) led to a water balance
 393 consistent with the groundwater level variation from October 2009 to September 2019. Mean
 394 annual rates in the study period: precipitation = 1403 mm/a; streamflow = 384 mm/a ($0.63 m^3/s$);
 395 baseflow = 324 mm/a ($0.54 m^3/s$); reference evapotranspiration = 1220 mm/a; and actual
 396 evapotranspiration = 985 mm/a. Horizontal lines indicate initial values.

397

398 3.2 Synthetic Time Series

399 The methods were effective to characterize the time delay mechanisms that generated the
 400 synthetic time series W (derived from a summation function) and Z (derived from a convolution
 401 operation), as shown in Figures 3 and 4. When the p-value (GC) is greater than 0.05 (adopted
 402 significance level), there is statistical evidence that the lagged time series does not present a
 403 causal relationship in the Granger sense. Complementary, the intensity of the functional
 404 connectivity, or causal interaction, between the lagged time series is proportional to the NMI
 405 metric. When the results are analyzed simultaneously, we realize that they were capable to
 406 identify the time lags in practically all instances. Exceptions happened for the cases in which
 407 large noise variances were used to generate the response time series (Figure 3i, Figure 4i),
 408 affecting especially the mutual information-based method. GC worked well for most of the
 409 cases. The most relevant inconsistencies were found in Figure 3c and Figure 3l, situations in

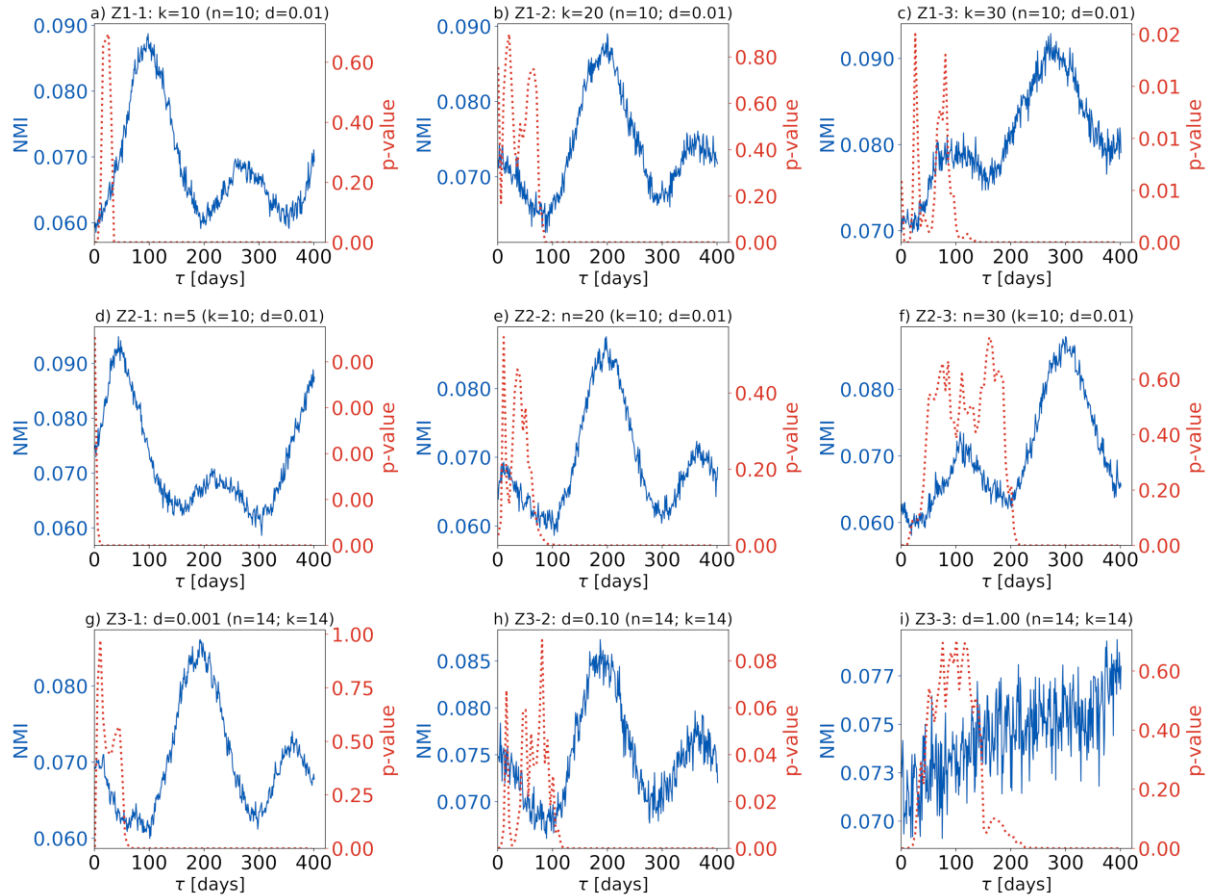
410 which the causal relationships in the Granger sense were identified for time lags about 100 and
 411 400 days, respectively, shorter than they should be.
 412
 413



414

415 **Figure 3.** Causal detection in the synthetic time series *W*. For the Granger causality analysis
 416 (GC, results indicated by the dotted red lines), the null hypothesis (absence of causal interaction
 417 in the Granger sense) is rejected when $p\text{-value} < 0.05$. The normalized time-lagged mutual
 418 information NMI (indicated by the blue lines) shows the functional connectivity dynamics
 419 between the time series (PP and W_j). The time lags in which global peaks occur correspond to
 420 the time lags (τ^*) used to generate the synthetic time series. In most of the instances, the GC and
 421 NMI methods correctly detected the time lags τ^* . The exceptions are found in plots *c*, *i* and *l*.

422



423

424 **Figure 4.** Causal detection in the synthetic time series Z. The NMI metric correctly detected in
 425 most of the cases the mean time-delay ($n.k$) of the unit hydrographs used to generate the time
 426 series, while the Granger causality analysis detected the causal relationships (p -value < 0.05)
 427 with some anticipation (between 50 and 150 days).

428

429 The Granger causality test, despite being designed to detect linear causal relationships,
 430 was capable to identify the lags in series W2-1, W2-2 and W2-3, in which non-linear functions
 431 of PP were used.

432

433 3.3 Observed Time Series

434 The Granger causality (GC) test confirmed that meteorological variables are influencing
 435 groundwater levels (GWL) and streamflow (total or baseflow) for practically all cases, with
 436 different time lags. A summary of the results is presented in Table 3. The precipitation affects (p -
 437 value < 0.05) the streamflow and the water level at practically all monitoring wells, even for
 438 short time lags (starting from 1 day). A singular behavior was found in the deepest water table
 439 (well W9), in which the causal interaction between precipitation and water level started to be
 440 confirmed only for time lags greater than 150 days.

441 Each well presented a unique GC response to evapotranspiration, regardless of the
 442 surrounding land cover, suggesting that the water table depth and the soil properties are together
 443 controlling the minimum time lag required to detect a causal interaction.

444 When analyzed as a response of the precipitation or as a cause of groundwater level
 445 changes, the EVI presented two disconnected intervals with p-value < 0.05.

446 Similarly to the presented for the synthetic time series, GC analysis only determines
 447 whether a causal interaction exists between time series, identifying the time-delay associated
 448 with them. As an additional source of information, the NMI measure shows details related to the
 449 strength and dynamics of functional connectivities between processes.

450

451 **Table 3.** Results of the Granger causality.

Causal interaction		Time lag intervals with p-value < 0.05 (M = 1000 days)
Cause	Response	
PP →	Q or Q _b	[1, M]
	GWL _j (j = 4, 5, 13, 14, 15, 16, 19)	[1, M]
	GWL ₉	[150, M]
	EVI	[1, 50] ∪ [265, M]
AET →	Q	[1, M]
	Q _b	[100, M]
	GWL ₁₄	[1, M]
	GWL _{4,16}	[10, M]
	GWL ₅	[20, M]
	GWL _{13, 15}	[30, M]
	GWL ₁₉	[100, M]
EVI →	Q	[300, M]
	Q _b	[370, M]
	GWL _{mean}	[1, 30] ∪ [270, M]
GWL →	Q or Q _b	[1, M]

452

453

454 Figure 5 presents NMI curves considering precipitation and evapotranspiration as causes
 455 and the groundwater levels as responses. To facilitate the visualization, simple moving averages
 456 of the NMI values, with a time period of 5 days, were plotted. The upwards trend observed in
 457 most of the curves occurs because the time-lagged mutual information, unlike GC analysis, does
 458 not eliminate the effects induced by the own response time series memory (dependency on
 459 previous states).

460 The results were examined individually. Considering first the precipitation, the wells W4
 461 and W5, which are 30 m apart and installed in a pasture area, presented a similar pattern despite
 462 the depth difference (~10 m, Table 1). This suggests that location and soil characteristics may be
 463 a critical factor to understand the results because they are monitoring different aquifers (mean
 464 water level equal to 16.5 m b.g.l. at W4, and 6.3 m b.g.l. at W5). The earliest local NMI peaks

465 occurred at 240 and 140 days for W4 and W5, respectively. These time lags seem to be related to
466 the mean time required to the water reach the respective water tables.

467 Only the well W9 did not present statistically significant NMI. That well is located out of
468 the watershed, 500 m away from the water divide and surrounded by a Eucalyptus plantation.
469 The great depth of the water table (20.2 m b.g.l., Table 1) may be one of the reasons that
470 contributed to the singular behavior.

471 The wells W13 and W14, 100 m apart in a sugarcane crop area, followed a similar
472 general shape, with the earliest NMI peaks at 100 and 75 days.

473 The well W15, located in a citrus orchard, presented a trending NMI curve, without any
474 relevant peaks. For the wells W16 and W19, which are in a Eucalyptus plantation area and
475 located 150 and 500 m away from the Onça Creek (main stream), the NMI curves showed
476 similar patterns, with earliest local (and global) peaks at 115 and 175 days, respectively.

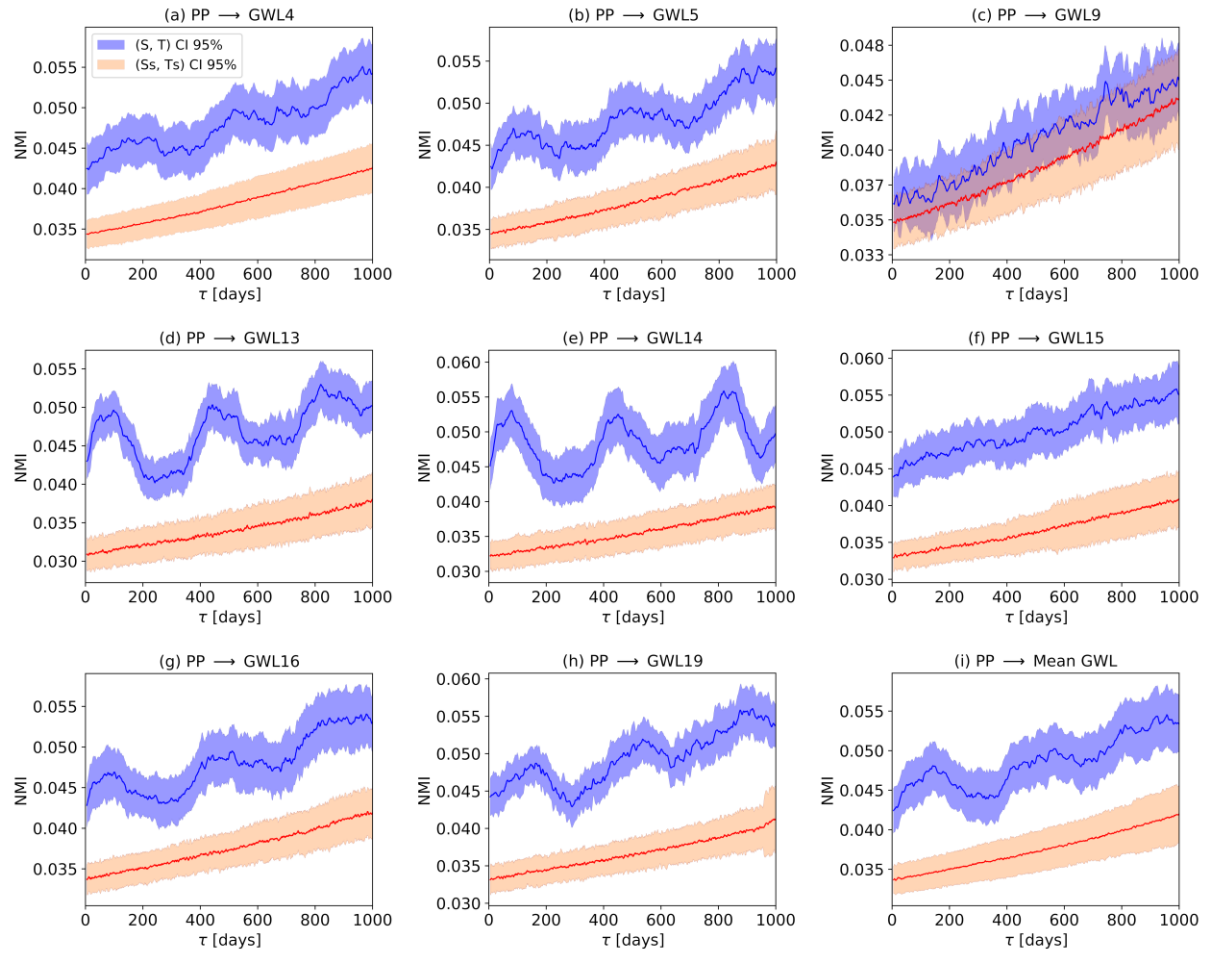
477 When examining the interaction between groundwater levels and evapotranspiration
478 (AET) (Figure 6), the water levels at wells close to each other (W4 and W5; W13 and W14; W16
479 and W19) exhibited similar NMI patterns. Such patterns are characterized by multiple local
480 peaks, which overall did not coincide with the peaks found in the analyses with precipitation.

481 When comparing the time lags in which local NMI peaks occurred with those lags
482 detected by the GC analysis (Table 3), no wells showed inconsistency, that is, all peaks occurred
483 in intervals with causal interaction confirmed in the Granger sense.

484

485

486



487

488 **Figure 5.** Normalized time-lagged mutual information (NMI) of the interaction between
 489 precipitation (PP) and groundwater level at the monitoring wells (GWL_j) for time delays (τ) up to
 490 1000 days. (S, T): indicates the NMI curves for the source (cause) and target (response)
 491 variables, generated using their respective mean values and uncertainties, and (Ss, Ts): indicates
 492 the NMI curves for the shuffled time series.

493

494

495

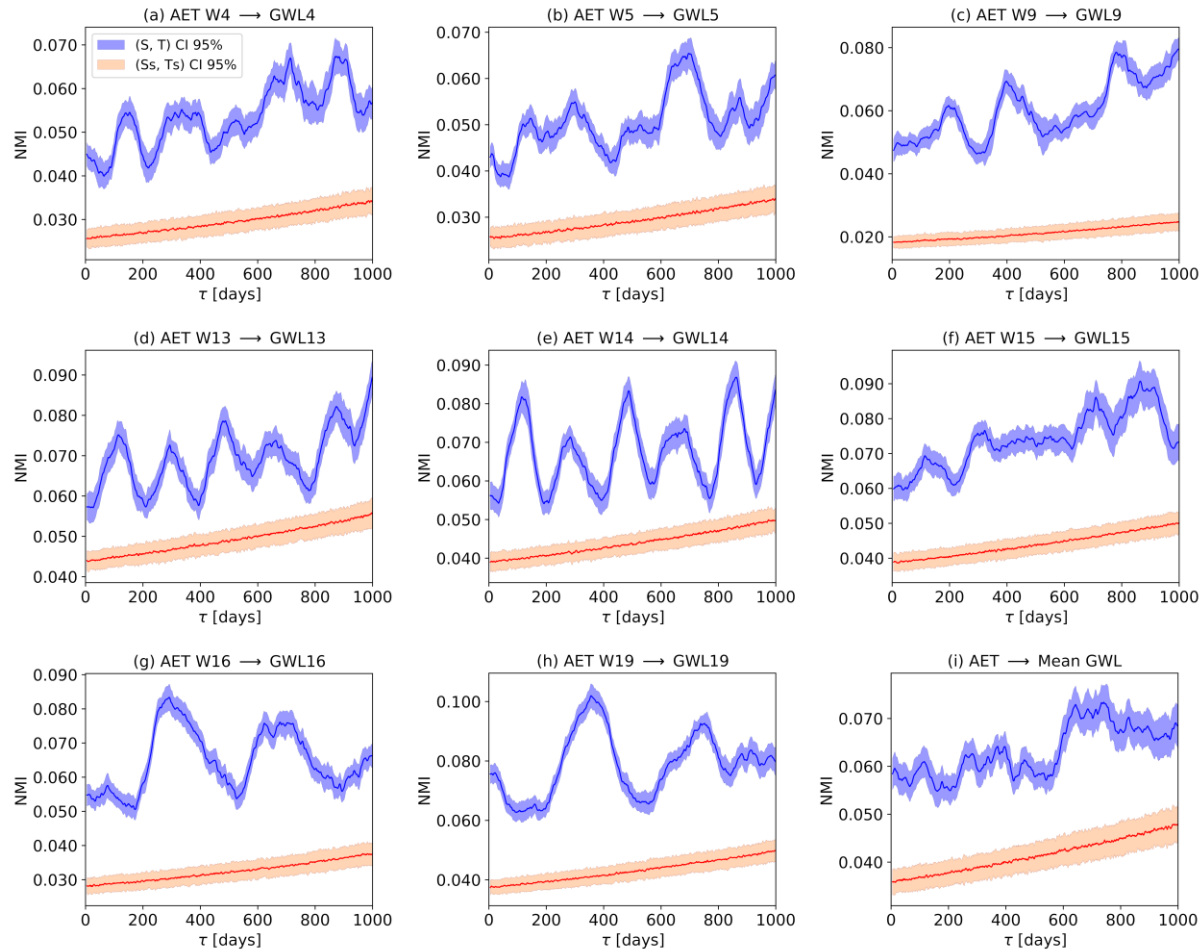
496

497

498

499

500



501

502 **Figure 6.** Normalized time-lagged mutual information (NMI) of the interaction between
 503 evapotranspiration (AET) and groundwater level at the monitoring wells (GWL_j) for time delays
 504 (τ) up to 1000 days. (S, T): indicates the NMI curves for the source (cause) and target (response)
 505 variables, generated using their respective mean values and uncertainties, and (Ss, Ts): indicates
 506 the NMI curves for the shuffled time series.

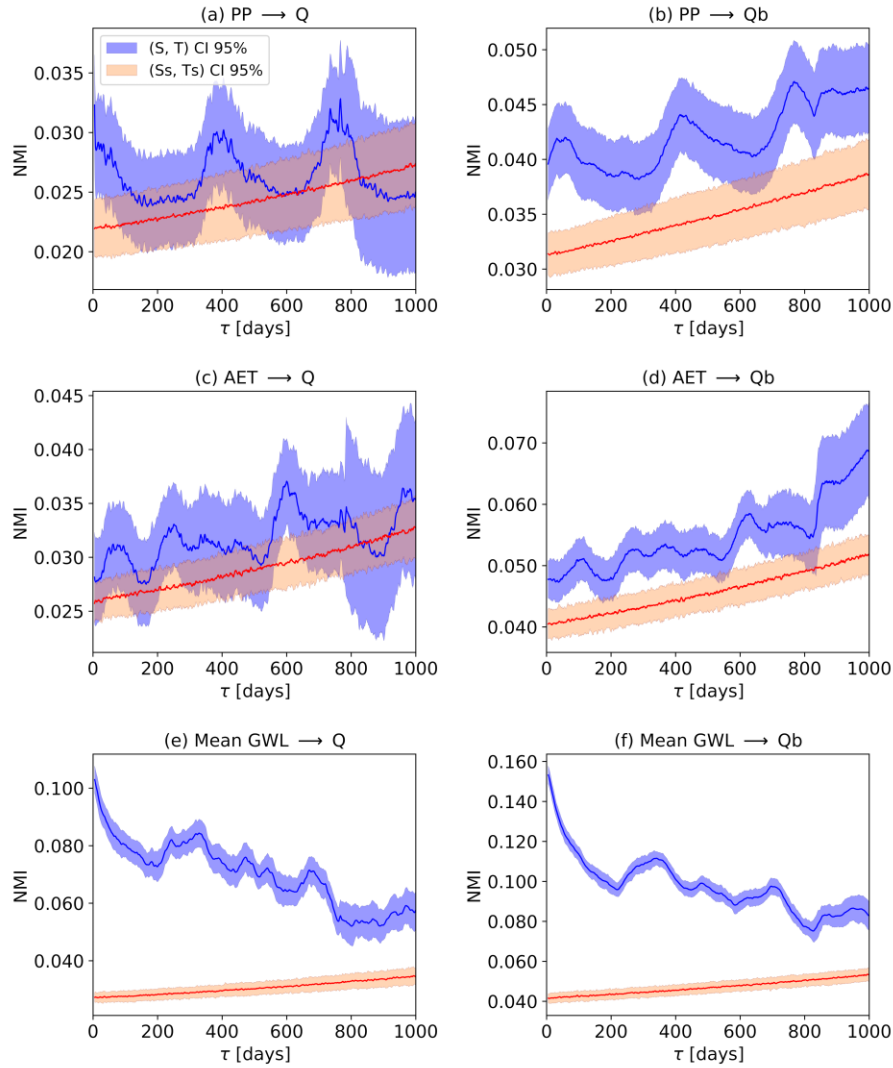
507

508 Figure 7 shows how precipitation, evapotranspiration, EVI and mean GWL interact with
 509 total streamflow (a) and baseflow (b) over different time delays. The hydraulic connectivity
 510 between the aquifer and the stream is evidenced by the high NMI values for early time lags. The
 511 NMI curve for the relationship between precipitation and streamflow drops rapidly in the first 5
 512 days of delay, and it develops two local peaks at 380 and 765 days. The NMI curve for the
 513 baseflow as a response of the precipitation presented local maxima at 50, 415, 780, and 845 days.
 514 The evapotranspiration presented slight peaks every ~ 180 days.

515

516

517



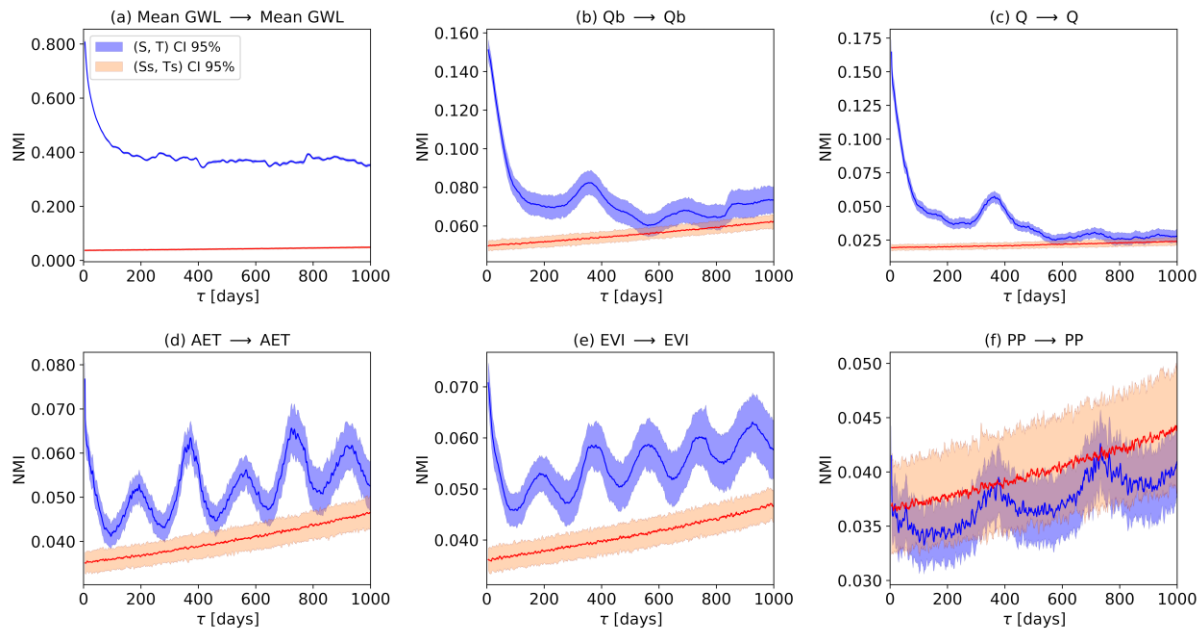
518

519 **Figure 7.** NMI metric between meteorological/vegetation forcings (precipitation-PP, reference
 520 evapotranspiration-RET, enhanced vegetation index-EVI, estimated actual evapotranspiration-
 521 AET) or groundwater states (mean groundwater level-GWL) and streamflow (Q) and baseflow
 522 (Qb) responses. (S, T): indicates the NMI curves for source (cause) and target (response)
 523 variables, generated using their respective mean values and uncertainties, and (Ss, Ts): indicates
 524 the NMI curves for the shuffled time series.

525

526 To support the interpretation of the results showed in Figures 5, 6 and 7, especially to
 527 better know the memory timescale and the persistence of the hydrological processes, the time-
 528 lagged mutual information was also calculated for each variable, determining a ‘self-
 529 information’ (Figure 8). Notably, the mean groundwater level (GWL) has the highest
 530 persistence, followed by the baseflow and streamflow. The memory timescale, if estimated by
 531 the first local minimum of the time-lagged mutual information, was about 200 days for GWL, Q,
 532 and Q_b, and about 100 days for EVI and AET. The precipitation did not present statistically
 533 significant results.

534



535

536 **Figure 8.** Time-lagged mutual information series comparing each variable to itself at various
 537 lags. (S, T): indicates the NMI curves for source (cause) and target (response) variables,
 538 generated using their respective mean values and uncertainties, and (Ss, Ts): indicates the NMI
 539 curves for the shuffled time series.

540

541 4 Discussion

542 The time-lagged mutual information and the Granger causality test proved to be effective
 543 to detect relevant time lags in synthetic time series. Simple and convergent interpretations were
 544 possible in our assessment. When analyzing the watershed data, however, the results were
 545 diverse, without a clear pattern. The Granger test seemed to be useful to detect processes that
 546 demand a large time delay to establish a connection. Since our study area is relatively small (~
 547 52 km²), in most of the cases, the causal interaction was detected even for 1-day lag (Table 3).
 548 These results could be expected since all local processes are structurally connected, sometimes
 549 with an intermediate reservoir (e.g., soil). Nevertheless, the innovative information we obtain
 550 from them is very limited. The NMI curves presented multiple and statistically significant local
 551 peaks, which are likely attributed to the memory of the response time series itself (Li et al.,
 552 2017). The causal information flow may be limited only to the first local peak, mainly when we
 553 try to give a physical interpretation. For example, the results from the pairs formed by
 554 precipitation and groundwater level (Figure 5) suggest that the first peak is the mean time
 555 required for the rainwater to reach the water table, while the second and third peaks are products
 556 of the seasonality of the variables. The diversity of patterns in the NMI curves also suggest that
 557 location, soil characteristics and land cover are all contributing to the responses of groundwater
 558 levels. Streamflow is highly dependent on the groundwater (Figure 7), validating the physical
 559 knowledge (or conceptual model) we have about the system (Machado et al., 2016; Wendland et
 560 al., 2015).

561 For the same watershed studied here, the study by Gómez et al. (2018) applied correlation
562 and wavelet transform based techniques and found a response time of approximately 2 years of
563 the baseflow to precipitation events. This result seems to correspond to that presented in Figure
564 6b (global NMI peak at ~750 days). Nevertheless, when considering the general upwards trend
565 of the mutual information observed in practically all pairwise analyses, we understand that only
566 the first local peak has a potential physical meaning related to response time, whereas the other
567 peaks are associated with the auto dependency found in the precipitation data (Figure 8f) or in
568 other driving variables. This interpretation is reinforced by the groundwater level responses to
569 precipitation (Figure 5) once the first NMI peaks occur in the same range of 50 to 100 days of
570 time lag. We noticed the importance of using different methods, as suggested by Rinderer et al.
571 (2018), to characterize data interdependencies and minimize subjectivity in the interpretations.

572 Although the interactions in the hydrologic system are generally nonlinear, the Granger
573 causality test revealed the existence of causal interactions in most of the pairwise analyses, even
574 for very short time lags. Similar capability of detecting nonlinear dependencies in
575 hydrometeorological systems using the Granger test was reported by Ombadi et al. (2020). In our
576 case, the detections may have been facilitated by the high connectivity between the hydrological
577 processes. In some instances, the Granger test was useful to detect low connectivity between
578 causes and responses (e.g., GWL9). We did not find a clear pattern in the results that could be
579 associated with a physical interpretation of the lags detected. Although the Granger causality test
580 seems to not be as useful as other information theoretic-based methods when assessing the
581 connectivity between processes, it still provides some information. One utility we defend is
582 precisely the opportunity to reduce uncertainties related to the interpretations. For example, a
583 local peak in the NMI curve between the variables S and T for a time lag in which there is no
584 causality in the Granger sense possibly will not have a relevant meaning.

585

586 4.1 Limitations and Future Directions

587 This study consists of a practical application of causal analysis to a hydrologic system.
588 The meaning of the multiple peaks of the NMI measure and the possible physical interpretation
589 associated with the results require further clarification. Even in a scenario with doubts about
590 these meanings and interpretations, we understand that the methods have potential to show
591 relevant characteristics of the hydrologic system behavior and could be useful for the
592 development and evaluation of models.

593 The reproduction of hydrologic responses and their time-lagged dependencies
594 (connectivity) with driving variables seems to be an attractive criterion to be considered in
595 future research. Time lagged mutual information (with the issues related to the memory effects),
596 or even a more complex measure such as the transfer entropy (Bennett et al., 2019), may serve as
597 an additional metric to evaluate the consistency and adequacy of hydrologic models.

598 Another potential application based on the results here presented refer to the construction
599 of tools for real-time streamflow forecasts because many of these tools use a combination of
600 lagged precipitation and streamflow data to perform the predictions (Gómez et al., 2019;
601 Jahandideh-Tehrani et al., 2020; Lv et al., 2020). Mutual information measures can be useful to
602 define the ‘optimal’ time lags to be considered.

603 Our dataset is relatively short (10 years of daily data) to detect eventual variations in the
604 way that the hydrologic variables interact with each other over time, such as done in the study by
605 Franzen et al. (2020). Undoubtedly, understanding how connectivity measures change over time
606 and how environmental changes (e.g., land use, climate variability) influence the connectivity
607 between hydrological processes are relevant topics to be addressed in future studies.

609 **5 Conclusions**

610 Two causal discovery methods (Granger's causality and mutual information) were
611 assessed and used to characterize pairwise time-lagged dependencies of daily data observed in a
612 small sub-tropical watershed. The water balance closure was verified considering the
613 groundwater storage dynamics. Unsurprisingly, statistically significant causal interactions were
614 confirmed between most of the water balance components. The analysis conducted allowed us to
615 characterize temporal interdependencies with long time windows, to identify some patterns, to
616 explore the strength of connectivity between hydrological processes, and to estimate the memory
617 timescale of variables.

618 Despite these capabilities, further studies are required to constrain the possible
619 interpretations and to create a connection between statistical results and the hydrologic system
620 dynamics. The option of using data from a watershed, an open system with many associated
621 uncertainties, and insufficient characterization, made it unfeasible to advance in that sense. This
622 is an opportunity, however, to advance combined field hydrology and modeling studies to move
623 from abstract statistical results to objective physical interpretations.

624 Throughout this paper, the potential of causal methods in characterizing the connectivity
625 between variables was evidenced. Real-world applications, with examples of how such methods
626 can contribute to hydrological science and applied hydrology, considering data limitations, seem
627 to be essential to engage the community. In future studies, one can test, for instance, if a model
628 accurately reproduces the connectivity patterns found in observed data, even when the reasons
629 behind the patterns are unknown. Similar approaches can improve the adequacy and performance
630 of predictive tools and constrain uncertainties.

633 **Data Availability**

634
635 Hydrologic data used in this research is publicly available at
636 <https://github.com/kalylgc/causebro/tree/Data/>
637
638

639 **References**

- 640 Allen, R. G. (1998). FAO Irrigation and Drainage Paper Crop by. *Irrigation and Drainage*,
641 300(56), 300. <https://doi.org/10.1016/j.eja.2010.12.001>
- 642 Alvares, C. A., Stape, J. L., Sentelhas, P. C., De Moraes Gonçalves, J. L., & Sparovek, G.
643 (2013). Köppen's climate classification map for Brazil. *Meteorologische Zeitschrift*, 22(6),
644 711–728. <https://doi.org/10.1127/0941-2948/2013/0507>

- 645 Amblard, P. O., & Michel, O. J. J. (2013). The relation between granger causality and directed
646 information theory: A review. *Entropy*, *15*(1), 113–143. <https://doi.org/10.3390/e15010113>
- 647 Araújo, L. M., França, A. B., & Potter, P. E. (1999). Hydrogeology of the Mercosul aquifer
648 system in the Paraná and Chaco-Paraná Basins, South America, and comparison with the
649 Navajo-Nugget aquifer system, USA. *Hydrogeology Journal*, *7*(3), 317–336.
650 <https://doi.org/10.1007/s100400050205>
- 651 Barnett, L., & Seth, A. K. (2015). Granger causality for state-space models. *Physical Review E -*
652 *Statistical, Nonlinear, and Soft Matter Physics*, *91*(4), 1–5.
653 <https://doi.org/10.1103/PhysRevE.91.040101>
- 654 Barnett, L., Barrett, A. B., & Seth, A. K. (2009). Granger causality and transfer entropy Are
655 equivalent for gaussian variables. *Physical Review Letters*, *103*(23), 2–5.
656 <https://doi.org/10.1103/PhysRevLett.103.238701>
- 657 Batista, L. V., Gastmans, D., Sánchez-Murillo, R., Farinha, B. S., dos Santos, S. M. R., & Kiang,
658 C. H. (2018). Groundwater and surface water connectivity within the recharge area of
659 Guarani aquifer system during El Niño 2014–2016. *Hydrological Processes*, *32*(16), 2483–
660 2495. <https://doi.org/10.1002/hyp.13211>
- 661 Bennett, A., Nijssen, B., Ou, G., Clark, M., & Nearing, G. (2019). Quantifying Process
662 Connectivity With Transfer Entropy in Hydrologic Models. *Water Resources Research*,
663 *55*(6), 4613–4629. <https://doi.org/10.1029/2018WR024555>
- 664 Besbes, M., & De Marsily, G. (1984). From infiltration to recharge: use of a parametric transfer
665 function. *Journal of Hydrology*, *74*(3–4), 271–293. [https://doi.org/10.1016/0022-](https://doi.org/10.1016/0022-1694(84)90019-2)
666 [1694\(84\)90019-2](https://doi.org/10.1016/0022-1694(84)90019-2)
- 667 Blöschl, G., Bierkens, M. F. P., Chambel, A., Cudennec, C., Destouni, G., Fiori, A., et al. (2019).
668 Twenty-three unsolved problems in hydrology (UPH)—a community perspective.
669 *Hydrological Sciences Journal*, *64*(10), 1141–1158.
670 <https://doi.org/10.1080/02626667.2019.1620507>
- 671 Cabrera, M. C. M., Anache, J. A. A., Youlton, C., & Wendland, E. (2016). Performance of
672 evaporation estimation methods compared with standard 20 m² tank. *Revista Brasileira de*
673 *Engenharia Agrícola e Ambiental*, *20*(10), 874–879. [https://doi.org/10.1590/1807-](https://doi.org/10.1590/1807-1929/agriambi.v20n10p874-879)
674 [1929/agriambi.v20n10p874-879](https://doi.org/10.1590/1807-1929/agriambi.v20n10p874-879)
- 675 Coelho, C. A. S., de Oliveira, C. P., Ambrizzi, T., Reboita, M. S., Carpenedo, C. B., Campos, J.
676 L. P. S., et al. (2016). The 2014 southeast Brazil austral summer drought: regional scale
677 mechanisms and teleconnections. *Climate Dynamics*, *46*(11–12), 3737–3752.
678 <https://doi.org/10.1007/s00382-015-2800-1>
- 679 Coutinho, J. V., Porsani, J. L., Elis, V. R., Santos, V. R. N., Ustra, A. T., & Wendland, E. (2020).
680 Applications of geophysical techniques to improve a groundwater conceptual model in an
681 outcrop area of the Guarani Aquifer System, in Brazil. *Environmental Earth Sciences*,
682 *79*(18), 1–11. <https://doi.org/10.1007/s12665-020-09163-4>
- 683 Cover, T. M., & Thomas, J. A. (2005). *Elements of Information Theory* (2nd ed.), Hoboken, NJ:
684 John Wiley & Sons Inc. <https://doi.org/10.1002/047174882X>

- 685 Dey, P., & Mujumdar, P. P. (2018). Multiscale evolution of persistence of rainfall and
686 streamflow. *Advances in Water Resources*, *121*(August), 285–303.
687 <https://doi.org/10.1016/j.advwatres.2018.08.018>
- 688 Didan, K. (2015). MOD13Q1 MODIS/Terra Vegetation Indices 16-Day L3 Global 250m SIN
689 Grid V006 [Data set]. NASA EOSDIS Land Processes DAAC. Accessed 2020-11-23 from
690 <https://doi.org/10.5067/MODIS/MOD13Q1.006>
- 691 Dirks, K. N., Hay, J. E., Stow, C. D., & Harris, D. (1998). High-resolution studies of rainfall on
692 Norfolk Island Part II : Interpolation of rainfall data. *Journal of Hydrology*, *208*(3-4), 187–
693 193. [https://doi.org/10.1016/S0022-1694\(98\)00155-3](https://doi.org/10.1016/S0022-1694(98)00155-3)
- 694 Donohue, R. J., Roderick, M. L., & McVicar, T. R. (2007). On the importance of including
695 vegetation dynamics in Budyko's hydrological model. *Hydrology and Earth System
696 Sciences*, *11*(2), 983–995. <https://doi.org/10.5194/hess-11-983-2007>
- 697 Duncan, H. P. (2019). Baseflow separation – A practical approach. *Journal of Hydrology*, *575*,
698 308–313. <https://doi.org/10.1016/j.jhydrol.2019.05.040>
- 699 Franzen, S. E., Farahani, M. A., & Goodwell, A. E. (2020). Information Flows: Characterizing
700 Precipitation-Streamflow Dependencies in the Colorado Headwaters With an Information
701 Theory Approach. *Water Resources Research*, *56*(10), 1–17.
702 <https://doi.org/10.1029/2019WR026133>
- 703 Fraser, A. M., & Swinney, H. L. (1986). Independent coordinates for strange attractors from
704 mutual information. *Physical Review A*, *33*(2), 1134–1140.
705 <https://doi.org/10.1103/PhysRevA.33.1134>
- 706 Freedman, D., & Diaconis, P. (1981). On the histogram as a density estimator:L2 theory.
707 *Zeitschrift Für Wahrscheinlichkeitstheorie Und Verwandte Gebiete*, *57*(4), 453–476.
708 <https://doi.org/10.1007/BF01025868>
- 709 Gençağa, D. (2018). Transfer entropy. *Entropy*, *20*(4), 1–4. <https://doi.org/10.3390/e20040288>
- 710 Glenn, E. P., Neale, C. M. U., Hunsaker, D. J., & Nagler, P. L. (2011). Vegetation index-based
711 crop coefficients to estimate evapotranspiration by remote sensing in agricultural and
712 natural ecosystems. *Hydrological Processes*, *25*(26), 4050–4062.
713 <https://doi.org/10.1002/hyp.8392>
- 714 Gómez, D., Melo, D. C. D., Rodrigues, D. B. B., Xavier, A. C., Guido, R. C., & Wendland, E.
715 (2018). Aquifer Responses to Rainfall through Spectral and Correlation Analysis. *Journal
716 of the American Water Resources Association*, *54*(6), 1341–1354.
717 <https://doi.org/10.1111/1752-1688.12696>
- 718 Gómez, D., Wendland, E., & Melo, D. C. D. (2020). Empirical rainfall-based model for defining
719 baseflow and dynamical water use rights. *River Research and Applications*, *36*(2), 189–198.
720 <https://doi.org/10.1002/rra.3565>
- 721 Goodwell, A. E., & Kumar, P. (2017). Temporal information partitioning: Characterizing
722 synergy, uniqueness, and redundancy in interacting environmental variables. *Water
723 Resources Research*, *53*(7), 5920-5942. <http://doi.org/10.1002/2016WR020216>
- 724 Goodwell, A. E., Jiang, P., Ruddell, B. L., & Kumar, P. (2020). Debates—Does Information

- 725 Theory Provide a New Paradigm for Earth Science? Causality, Interaction, and Feedback.
726 *Water Resources Research*, 56(2), 1–12. <https://doi.org/10.1029/2019WR024940>
- 727 Granger, C. J. W. (1969). Investigating Causal Relations by Econometric Models and Cross-
728 spectral Methods. *Econometrica*, 37(3), 424–438. <https://doi.org/10.2307/1912791>
- 729 Graves, T., Gramacy, R., Watkins, N., & Franzke, C. (2017). A brief history of long memory:
730 Hurst, Mandelbrot and the road to ARFIMA, 1951-1980. *Entropy*, 19(9), 1–21.
731 <https://doi.org/10.3390/e19090437>
- 732 Huang, X., Maçaira, P. M., Hassani, H., Cyrino Oliveira, F. L., & Dhesi, G. (2019). Hydrological
733 natural inflow and climate variables: Time and frequency causality analysis. *Physica A:
734 Statistical Mechanics and Its Applications*, 516, 480–495.
735 <https://doi.org/10.1016/j.physa.2018.09.079>
- 736 Jiang, P., & Kumar, P. (2019). Information transfer from causal history in complex system
737 dynamics. *Physical Review E*, 99(1), 1–13. <https://doi.org/10.1103/PhysRevE.99.012306>
- 738 Kamble, B., Kilic, A., & Hubbard, K. (2013). Estimating crop coefficients using remote sensing-
739 based vegetation index. *Remote Sensing*, 5(4), 1588–1602.
740 <https://doi.org/10.3390/rs5041588>
- 741 Kirchheim, R. E., Gastmans, D., Chang, H. K., & Gilmore, T. E. (2019). The use of isotopes in
742 evolving groundwater circulation models of regional continental aquifers: The case of the
743 Guarani Aquifer System. *Hydrological Processes*, 33(17), 2266–2278.
744 <https://doi.org/10.1002/hyp.13476>
- 745 Kumar, P., & Gupta, H. V. (2020). Debates—Does Information Theory Provide a New Paradigm
746 for Earth Science? *Water Resources Research*, 56(2), 1–10.
747 <https://doi.org/10.1029/2019WR026398>
- 748 Li, S., Xu, J., Chen, G., Lin, L., Zhou, D., & Cai, D. (2017). The characterization of hippocampal
749 theta-driving neurons-A time-delayed mutual information approach. *Scientific Reports*,
750 7(1), 1–12. <https://doi.org/10.1038/s41598-017-05527-2>
- 751 Li, S., Xiao, Y., Zhou, D., & Cai, D. (2018). Causal inference in nonlinear systems: Granger
752 causality versus time-delayed mutual information. *Physical Review E*, 97(5), 1–9.
753 <https://doi.org/10.1103/PhysRevE.97.052216>
- 754 Lv, N., Liang, X., Chen, C., Zhou, Y., Li, J., Wei, H., & Wang, H. (2020). A long Short-Term
755 memory cyclic model with mutual information for hydrology forecasting: A Case study in
756 the xixian basin. *Advances in Water Resources*, 141(May).
757 <https://doi.org/10.1016/j.advwatres.2020.103622>
- 758 Machado, A. R., Wendland, E., & Krause, P. (2016). Hydrologic Simulation for Water Balance
759 Improvement in an Outcrop Area of the Guarani Aquifer System. *Environmental Processes*,
760 3(1), 19–38. <https://doi.org/10.1007/s40710-016-0128-4>
- 761 Marengo, J. A., Nobre, C. A., Seluchi, M. E., Cuartas, A., Alves, L. M., Mendiondo, E. M., et al.
762 (2015). A seca e a crise hídrica de 2014-2015 em São Paulo. *Revista USP*, (106), 31.
763 <https://doi.org/10.11606/issn.2316-9036.v0i106p31-44>
- 764 McGraw, M. C., & Barnes, E. A. (2018). Memory matters: A case for granger causality in

- 765 climate variability studies. *Journal of Climate*, 31(8), 3289–3300.
766 <https://doi.org/10.1175/JCLI-D-17-0334.1>
- 767 Nagler, P. L., Glenn, E. P., Nguyen, U., Scott, R. L., & Doody, T. (2013). Estimating riparian
768 and agricultural actual evapotranspiration by reference evapotranspiration and MODIS
769 enhanced vegetation index. *Remote Sensing*, 5(8), 3849–3871.
770 <https://doi.org/10.3390/rs5083849>
- 771 Ombadi, M., Nguyen, P., Sorooshian, S., & Hsu, K. lin. (2020). Evaluation of Methods for
772 Causal Discovery in Hydrometeorological Systems. *Water Resources Research*, 56(7), 1–
773 22. <https://doi.org/10.1029/2020WR027251>
- 774 Papagiannopoulou, C., Miralles, Di. G., Decubber, S., Demuzere, M., Verhoest, N. E. C.,
775 Dorigo, W. A., & Waegeman, W. (2017). A non-linear Granger-causality framework to
776 investigate climate-vegetation dynamics. *Geoscientific Model Development*, 10(5), 1945–
777 1960. <https://doi.org/10.5194/gmd-10-1945-2017>
- 778 Pelletier, J. D., & Turcotte, D. L. (1997). Long-range persistence in climatological and
779 hydrological time series: Analysis, modeling and application to drought hazard assessment.
780 *Journal of Hydrology*, 203(1–4), 198–208. [https://doi.org/10.1016/S0022-1694\(97\)00102-9](https://doi.org/10.1016/S0022-1694(97)00102-9)
- 781 Pompeo, C. A. (1990). Balanço hídrico da zona não-saturada do solo na bacia do Ribeirão da
782 Onça (SP), (Doctoral dissertation). São Carlos, SP: University of São Paulo.
- 783 Rinderer, M., Ali, G., & Larsen, L. G. (2018). Assessing structural, functional and effective
784 hydrologic connectivity with brain neuroscience methods: State-of-the-art and research
785 directions. *Earth-Science Reviews*, 178, 29–47.
786 <https://doi.org/10.1016/j.earscirev.2018.01.009>
- 787 Ruddell, B. L., & Kumar, P. (2009). Ecohydrologic process networks: 1. Identification. *Water*
788 *Resources Research*, 45(3), 1–23. <https://doi.org/10.1029/2008WR007279>
- 789 Runge, J., Bathiany, S., Bollt, E., Camps-Valls, G., Coumou, D., Deyle, E., et al. (2019).
790 Inferring causation from time series in Earth system sciences. *Nature Communications*,
791 10(1), 1–13. <https://doi.org/10.1038/s41467-019-10105-3>
- 792 Schreiber, T. (2000). Measuring information transfer. *Physical Review Letters*, 85(2), 461–464.
793 <https://doi.org/10.1103/PhysRevLett.85.461>
- 794 Seabold, S., & Perktold, J. (2010). Statsmodels: Econometric and Statistical Modeling with
795 Python. *Proceedings of the 9th Python in Science Conference*, (SciPy), 92–96.
796 <https://doi.org/10.25080/majora-92bf1922-011>
- 797 Singh, N. K., & Borrok, D. M. (2019). A Granger causality analysis of groundwater patterns
798 over a half-century. *Scientific Reports*, 9(1), 1–8. <https://doi.org/10.1038/s41598-019-49278-8>
- 800 Tomasella, J., Hodnett, M.G., Cuartas, L.A., Nobre, A.D., Waterloo, M.J., & Oliveira, S.M.
801 (2008). The water balance of an Amazonian micro-catchment: the effect of interannual
802 variability of rainfall on hydrological behaviour. *Hydrological Processes*, 22(13), 2133–
803 2147. <https://doi.org/10.1002/hyp.6813>
- 804 Wegehenkel, M. (2009). Modeling of vegetation dynamics in hydrological models for the

- 805 assessment of the effects of climate change on evapotranspiration and groundwater
806 recharge. *Advances in Geosciences*, 21, 109–115. [https://doi.org/10.5194/adgeo-21-109-](https://doi.org/10.5194/adgeo-21-109-2009)
807 2009
- 808 Weijs, S. V., Schoups, G., & Van De Giesen, N. (2010). Why hydrological predictions should be
809 evaluated using information theory. *Hydrology and Earth System Sciences*, 14(12), 2545–
810 2558. <https://doi.org/10.5194/hess-14-2545-2010>
- 811 Wendland, E., Barreto, C., & Gomes, L. H. (2007). Water balance in the Guarani Aquifer
812 outcrop zone based on hydrogeologic monitoring. *Journal of Hydrology*, 342(3–4), 261–
813 269. <https://doi.org/10.1016/j.jhydrol.2007.05.033>
- 814 Wendland, E., Gomes, L. H., & Troeger, U. (2015). Recharge contribution to the Guarani aquifer
815 system estimated from the water balance method in a representative watershed. *Anais Da*
816 *Academia Brasileira de Ciencias*, 87(2), 595–609. [https://doi.org/10.1590/0001-](https://doi.org/10.1590/0001-3765201520140062)
817 3765201520140062
- 818 Wilks, S. S. (1938). The Large-Sample Distribution of the Likelihood Ratio for Testing
819 Composite Hypotheses. *The Annals of Mathematical Statistics*, 9(1), 60–62.
820 <https://doi.org/10.1214/aoms/1177732360>
- 821 Zimmermann, B., Elsenbeer, H., & Moraes, J. M. (2006). The influence of land-use changes on
822 soil hydraulic properties: Implications for runoff generation. *Forest Ecology and*
823 *Management*, 222(1–3), 29–38. <https://doi.org/10.1016/j.foreco.2005.10.070>